Single-Channel Analysis of Inactivation-Defective Rat Skeletal Muscle Sodium Channels Containing the F1304Q Mutation

John H. Lawrence,*# David W. Orias,* Jeffrey R. Balser,§ H. Bradley Nuss,* Gordon F. Tomaselli,* Brian O'Rourke,* and Eduardo Marban*¶

Departments of *Medicine, #Pediatrics, §Anesthesiology and Critical Care Medicine, and ¶Physiology, The Johns Hopkins University School of Medicine, Baltimore, Maryland 21205 USA

ABSTRACT The intracellular linker between domains III and IV of the voltage-gated Na channel mediates fast inactivation. Targeted alteration of one or more of a triplet of hydrophobic amino acids within this linker region results in a marked slowing in the decay of ionic current. The mechanism of this defective inactivation was explored in rat skeletal muscle sodium channels (μ1) containing the F1304Q mutation in *Xenopus laevis* oocytes with and without coexpression of the rat brain β_1 subunit. Cell-attached single-channel patch-clamp recordings revealed that the μ1-F1304Q channel reopens multiple times with open times that are prolonged compared with those of the wild-type channel. Coexpression of the β_1 subunit stabilized a dominant nonbursting gating mode and accelerated the activation kinetics of μ1-F1304Q but did not modify mean open time or fast-inactivation kinetics. A Markov gating model incorporating separate fast- and slow-inactivation particles reproduced the results by assuming that the F1304Q mutation specifically influences transitions to and from fast-inactivated states. These effects are independent of interactions of the mutant channel with the β_1 subunit and do not result from a change in modal gating behavior. These results indicate that F1304Q mutant channels can still enter the inactivated state but do so reversibly and with altered kinetics.

INTRODUCTION

Voltage-gated sodium channels underlie the upstroke of the cellular action potential in cardiac and skeletal muscle and neuronal tissue. Within such excitable cells, sodium current is rapidly activated by membrane depolarization, but, with maintained depolarization over tens of milliseconds, the majority of this current inactivates completely. On the molecular scale, single-channel patch-clamp recordings demonstrate that individual sodium channels open briefly one or a few times in response to strong depolarizing voltage stimuli and then remain closed for the duration of the depolarizing voltage pulse (Aldrich et al., 1983; Vandenberg and Horn, 1984; Grant and Starmer, 1987; Yue et al., 1989). The final inactivating event appears to be mediated by an intracellular segment of the channel protein linking domains III and IV, referred to as the "inactivation gate," that occludes the inner mouth of the channel pore (Stühmer et al., 1989; Vassilev et al., 1988, 1989; Moorman et al., 1990; Patton et al., 1992; West et al., 1992). Translocation and subsequent docking of this gate to a hydrophobic receptor region within the pore (McPhee et al., 1994, 1995) results in a stable nonconducting (i.e., inactivated) state that persists until the membrane is repolarized and the inactivation gate is released.

A triplet of hydrophobic amino acids (isoleucine–phenylalanine–methionine) within the inactivation gate region appears to mediate binding of the gate to its receptor and thereby stabilizes the fast-inactivated state of the channel. Directed mutation of one or more of these amino acids to less hydrophobic residues results in markedly slowed inactivation of the sodium current in whole-cell experiments (West et al., 1992; Hartmann et al., 1994). The changes in macroscopic kinetics may result from removal of fast inactivation with retention of slow inactivation, destabilization of fast inactivation (i.e., no longer absorbing), or shifts in modal gating behavior. Only limited single-channel data are available to define precisely the nature of the defect in gating (West et al., 1992; Hartmann et al., 1994). To gain further insight into the molecular mechanisms underlying normal and defective sodium channel inactivation, we have employed single-channel patch-clamp recordings to examine the gating behavior of heterologously expressed rat skeletal muscle sodium channels with inactivation disrupted by a single amino acid mutation (F1304Q) within the III–IV linker region. A multistate gating model constructed from these records demonstrates that this mutation significantly influences only transitions to and from fast-inactivation states. These effects are not produced by changes in modal gating and are independent of a change in the interaction of this mutant channel with the β_1 subunit.

Received for publication 26 October 1995 and in final form 17 May 1996.

Address reprint requests to Dr. John H. Lawrence, Department of Medicine, Division of Cardiology, The Johns Hopkins University School of Medicine, Ross 844, 720 Rutland Avenue, Baltimore, MD 21205. Tel.: 410-955-2775; Fax: 410-955-7953; E-mail: jlawrenc@welchlink.welch.jhu.edu.

0006-3495/96/09/1285/10 $2.00

MATERIALS AND METHODS

Molecular biology and heterologous expression

An expression plasmid containing the full-length cDNA encoding the μ1 rat skeletal muscle sodium channel α subunit (Trimmer et al., 1989) was cloned into pGEM-9Zf(−) (Promega, Madison, WI). A 2.5-kb Sph 1–Kpn 1 restriction digest fragment from the μ1 cDNA encoding nucleotides 2230 to 4760 was subcloned into pGEM-7Zf(+) (Promega). In vitro site-di-

rected mutagenesis using uracil-containing DNA and phagemid vectors introduced a single amino substitution at position 1304, replacing phenylalanine for glutamine within the cytoplasmic linker between the third and fourth homologous domains of the sodium channel (Kunkel et al., 1987); this site lies in the center of three hydrophobic residues that appear to mediate fast inactivation of the sodium channel. The entire segment was sequenced by the dideoxy chain termination method (Sequenase, U.S. Biochemical, Cleveland, OH) and subcloned back into pGEM-9Zf(−) to form the full-length mutant sodium channel gene.

As previously described (Tomaselli et al., 1991), complementary RNA was prepared for both the wild-type and the mutant μ1 sodium channels and microinjected into freshly isolated mature *Xenopus laevis* oocytes. In some experiments, the rat brain sodium channel β_1 (Isom et al., 1992, 1995) cRNA was coinjected with the α subunit cRNA at a molar ratio of 1:1. We refer to the wild-type channel as μ1 and to the mutant channel as μ1-F1304Q.

Electrophysiological recordings

Sodium channel currents were recorded at room temperature from oocytes in the cell-attached configuration 2–4 days after cRNA injection as previously described (Backx et al., 1992). Currents were measured with an integrating headstage (Axon Instruments, Burlingame, CA), sampled at 10 kHz and low-pass filtered (four-pole Bessel, −3 dB at 2 kHz). The pulse protocol involved holding potentials from −120 to −60 mV and test potentials from −60 to +10 mV at a repetition frequency of 0.67 Hz. The more positive holding potentials were used to avoid stacking of openings in multichannel patches during measurements of channel open times; the few remaining stacked openings were excluded from the analysis. The number of channels per patch was determined as the maximum number of stacked openings in response to depolarizations to −20 mV in long runs (>100 sweeps). The patch pipette contained (in mM) 140 NaCl, 1 $BaCl_2$, and 10 HEPES (pH 7.3). The bath solution consisted of (in mM) 140 KCl and 10 HEPES (pH 7.3).

Data analysis

Single-channel unitary current amplitudes were determined from fits to amplitude histograms. These histograms were generated from well-resolved single-channel openings chosen from several sweeps and fitted with normal Gaussian distributions by use of a nonlinear, least-squares minimization algorithm in Origin (Northampton, MA). The unitary current amplitude was determined as the difference between the means of the histograms for the baseline current and the open-channel current. For the wild-type channel at positive test potentials, openings were short and sometimes poorly resolved and resulted in amplitude histograms that underestimated the full unitary current amplitude. In these cases, a manual estimate of the current amplitude was made.

For subsequent analysis, single-channel records were corrected for leak currents and capacity transients by digital subtraction of smooth templates fitted to records with no openings. Most patches contained 1–3 sodium channels. An event detection scheme based on a half-height criterion (Colquhoun and Sigworth, 1983) was used to generate an idealized form of the current from which ensemble averages and histograms were constructed. Mean open time was determined as the time constant of the best single-exponential fit to the open time histogram (Origin).

Convolution analysis (Aldrich et al., 1983) was performed as previously described (Yue et al., 1989) to assess the frequency of reopenings. The convolution in the time domain of the first latency density function with the open time density function matches the open probability time course if a channel opens only once per depolarization epoch. For a channel that reopens one or more times, this convolution integral accounts for only a fraction of the total open probability and demonstrates the contribution of first openings to the ensemble.

Markov modeling

To examine the effect of the F1304Q mutation on the gating of the μ1 channel, we fitted ensemble-average currents obtained from selected patches to a gating model by a numerical approach. The model (Fig. 8 *A* below) was modified (Tomaselli et al., 1995) from that recently described by Kuo and Bean (1994) for sodium channel gating in rat hippocampal CA1 neurons so that our model included a second binding particle that was responsible for slow inactivation. The channel opens following activation of four independent and identical voltage sensors (rate constants $n\alpha$; n = 1–4) and a subsequent gating transition (rate constant γ). The open channel may close to the last closed state (rate constant δ) and to deeper closed states (rate constants $n\beta$; n = 1–4), to a fast inactivation state (I_1; rate constant k_4), or to a slow inactivation state (I_2; rate constant k_8). Inactivation may result from block of any state by a fast (rate constants k_2a^n; n = 1–4) or slow (rate constants k_6b^n; n = 1–4) inactivation particle, and the affinity of the channel for either particle increases as the channel activates. To satisfy microscopic reversibility, factors a (identical to those in Kuo and Bean (1994)) and b (derived in a manner analogous to that for a) were incorporated into the rate constants to account for changes in gating kinetics when an inactivation particle is bound. Although other modifications to the single-particle Kuo–Bean formulation (1994) may also account for slow inactivation, our model readily reproduced the kinetics of a slow-inactivation process that is heavily modulated by β_1 coexpression.

As previously described, the fitting algorithm determines a set of rate constants that minimize the difference between the calculated probability of open state occupancy and the measured open state probability (Balser et al., 1990a,b). From single-channel data recorded at −20 mV, we obtained the open probability by dividing the ensemble-average current by the single-channel current amplitude and the number of channels in the patch. A numerical integration method for solving stiff differential equations, LSODA (Hindmarsh, 1983; Petzold, 1983), was used to calculate the open state probability from a model consisting of a set of initial rate constant estimates. The sum of the rate constants for transitions out of the open state was constrained by the experimentally measured mean open time. Data from μ1 and μ1-F1304Q were fitted simultaneously to gating models that differed only in the values of the rate constants governing transitions to and from the fast-inactivated state (rate constants k_1, k_2, k_3, k_4). Data from μ1-F1304+β_1 were fitted by a similar model that was constrained by the measured mean open time and the μ1-F1304Q model rate constants for transitions to and from the fast-inactivated state (rate constants k_1, k_2, k_3, k_4). A modified Simplex algorithm (Nelder and Mead, 1965) for minimizing the residual sum of squares was utilized to compare the models to the patch ensemble open probabilities and to update the rate constants.

RESULTS

Single-channel recordings

Fig. 1 illustrates the single-channel behavior of the wild-type μ1 and mutant μ1-F1304Q channels expressed in *Xenopus* oocytes without coexpression of the β_1 subunit. Representative traces and ensemble averages are shown in response to step depolarizations to −60 and 0 mV, respectively, in cell-attached one-channel patches. The μ1 records (Fig. 1 *A*) demonstrated the expected mode 1 voltage-dependent gating pattern (Zhou et al., 1991). Qualitatively, the mutant μ1-F1304Q channel (Fig. 1 *C*) had a similar unitary conductance and first latency but had more reopenings and longer open times. Inspection of long-lasting patch recordings demonstrated that the μ1 channel exhibits modal gating behavior, consistent with previous observations (Zhou et al., 1991; Ji et al., 1994). Two gating modes were readily identified in each of three patches when μ1 was

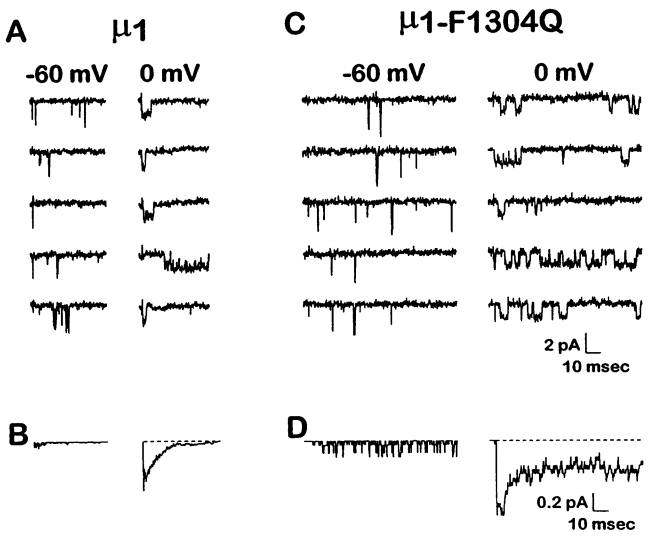

FIGURE 1 Single-channel recordings from cell-attached patches in *Xenopus* oocytes. Representative sweeps were selected from one-channel patches expressing μ1 (*A*) and μ1-F1304Q (*C*) sodium channels in response to depolarization from a holding potential of −120 mV to test potentials of −60 and 0 mV, respectively, for 100 ms. Although gating is not significantly altered at −60 mV, the mutant channel has more frequent channel reopenings and longer open times relative to the wild-type channel at 0 mV. Ensemble-average currents (*B, D*) demonstrate the delayed decay of peak current in the μ1-F1304Q channel compared with that in the μ1 channel.

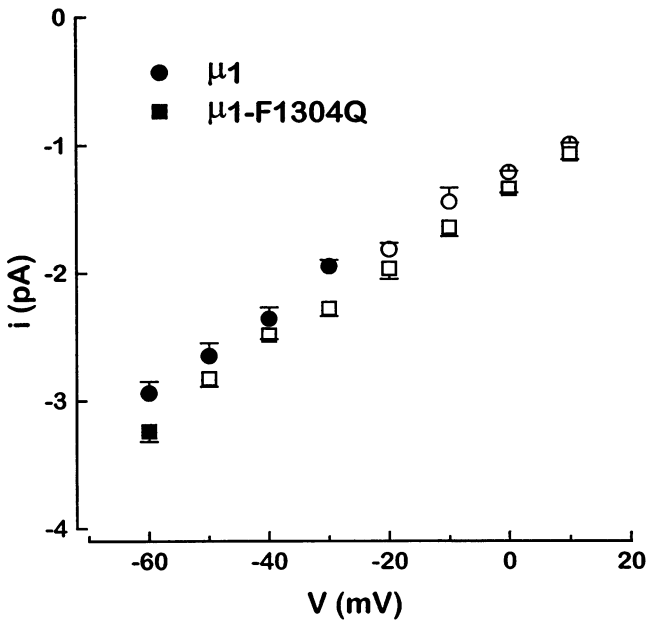

FIGURE 2 Unitary current amplitudes (*i*) from μ1 and μ1-F1304Q sodium channels at membrane potentials from −60 to 10 mV ($N \geq 3$ at each potential) determined from amplitude histograms (*open symbols*) where possible or by eye (*filled symbols*) when openings were brief. The slope conductance for μ1 was 28 ± 1 pS and for μ1-F1304Q was 30 ± 1 pS.

expressed in *Xenopus* oocytes. The dominant mode, referred to as mode 1, was distinguished by a rapid first latency and very infrequent reopenings. In contrast, in the less frequently observed mode, mode 2, the first openings were delayed (relative to mode 1 first latencies), and the channel reopened multiple times in a rapid bursting pattern.

Whereas ensemble average currents of the μ1 channel inactivated completely within 50 ms (Fig. 1 *B*), ensemble averages from the μ1-F1304Q channel decayed more slowly and incompletely, even at 100 ms (Fig. 1 *D*). These features were examined in greater detail, and the results are presented below.

Single-channel unitary current amplitudes (Fig. 2) were determined, when possible, from amplitude histograms (open symbols) from 3–6 patches at test potentials from −60 to +10 mV. At potentials where openings were quite brief, the amplitude histograms were not well fitted by Gaussian distributions and tended to underestimate the true unitary current amplitude. Therefore a best manual estimate (filled symbols) was made after inspection of the longest and best-resolved openings from many sweeps. The slope conductance for μ1 was 28 ± 1 pS and for F1304Q was 30 ± 1 pS. Thus, permeation is not altered by the F1304Q mutation.

Voltage-dependent gating

The most striking difference between the single-channel records of μ1 and μ1-F1304Q was in the number of channel openings/100 ms depolarization epoch at membrane potentials above −60 mV, as demonstrated in Fig. 1. The contribution of reopenings to the total current in μ1 and μ1-F1304Q patches during step depolarizations to −20 mV was assessed by convolution analysis, as shown in Fig. 3. The open time density function (τ_o) was convolved with the first latency density function (*f*) for both channel types and resulted in a function ($\tau_o * f$) that reflected the component of the current that was contributed by the initial openings in each sweep. For the μ1 channel this convolution closely approximates the open probability (p_o). This verifies that, at −20 mV, the wild-type channel usually opens only once before inactivating. For the μ1-F1304Q channel the convolution reproduced more than 90% of the peak open probability but fell far short of the subsequent open probability curve, indicating that channel reopenings were responsible for the persistent plateau of current in whole-cell and single-channel ensemble currents.

The second notable gating change in the mutant channel was a marked and progressive prolongation of mean open time relative to the μ1 channel at potentials above −60 mV (Fig. 4). Furthermore, whereas the μ1 channel demonstrated a shortening of open time above 0 mV, open times in the F1304Q channel approached a plateau rather than shortening at these potentials. Three to six patches were studied at each test potential.

Modal gating behavior

Fig. 5 summarizes data from a one-channel patch containing the μ1 channel depolarized to −20 mV for 50 ms. Two

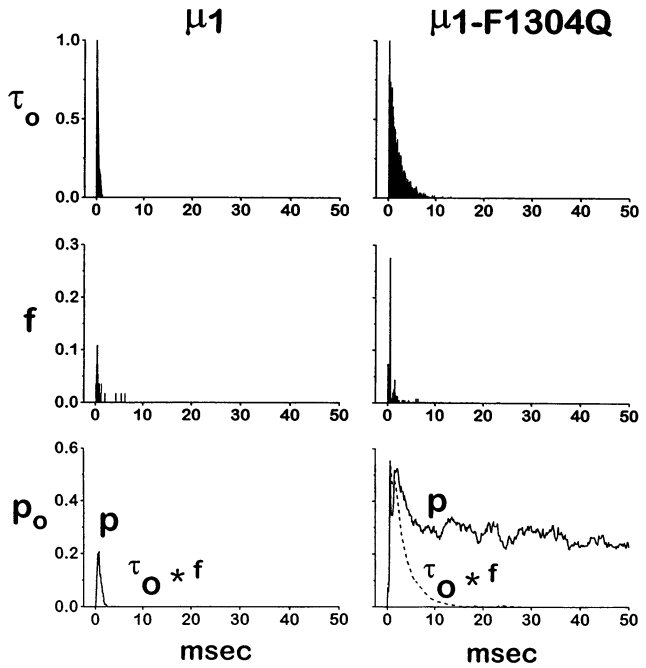

FIGURE 3 Convolution analysis of $\mu 1$ and $\mu 1$-F1304Q at membrane potential of -20 mV from a holding potential of -130 mV for $\mu 1$ and -120 mV for $\mu 1$-F1304Q. In the top row, τ_0 is the normalized open-time histogram. In the middle row, f is the first latency density function. In the bottom row, p is the open-channel probability computed as ensemble-average current normalized by the unitary current, and $\tau_0 * f$ is the convolution function.

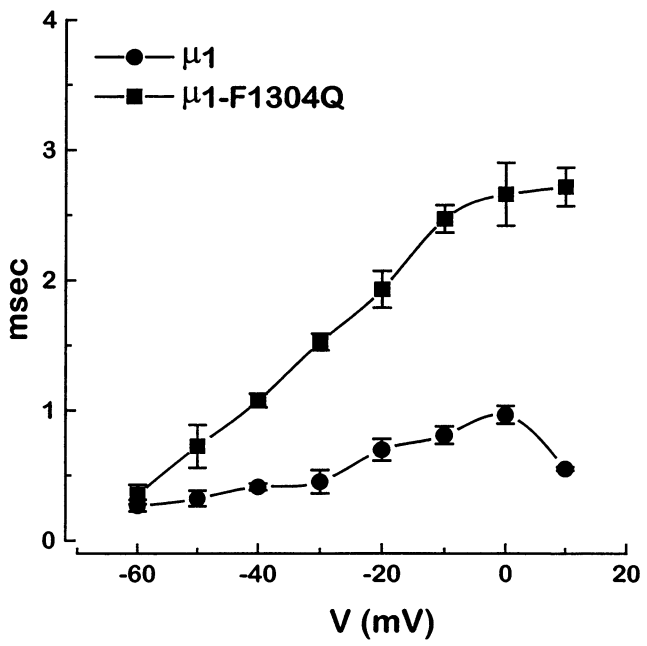

FIGURE 4 Mean open times (±SEM) as a function of membrane potential for $\mu 1$ and $\mu 1$-F1304Q ($N \geq 3$ at each potential) determined from open-time distributions fitted by single exponential functions. At each potential positive to -0 mV, the mean open time for $\mu 1$-F1304Q was significantly prolonged ($p < 0.05$) relative to $\mu 1$.

gating modes, distinguished by the presence or absence of bursting behavior at the beginning of the trace, were apparent by inspection of the single-channel records. Because of the variable length of the burst, parameters based simply on mean open or closed times did not reliably discriminate modes. Instead, a criterion was employed that specifically detected bursts. Sweeps that contained a burst, defined as three openings with a mean closed time of less than 1 ms, were placed in the burst mode. Although it is not a unique discriminator, this algorithm reliably sorted both the $\mu 1$ and the F1304Q channel activity. Fewer than 1% of sweeps were misclassified by the algorithm based on visual inspection of the records. In Fig. 5 *A* the mean burst closed time is shown for all sweeps with at least three openings; sweeps with one or two openings were automatically assigned to mode 1.

The initial 55 sweeps demonstrated primarily mode 2 bursting behavior, and the single-channel records from a subset of these traces are shown in Fig. 5 *B*. The ensemble-average current generated from all mode 2 sweeps activates slowly and decays gradually. After a quiescent period, scattered sweeps with multiple openings are seen and followed by a gating change near sweep 225 to predominantly mode 1 behavior. Representative sweeps shown in Fig. 5 *C* demonstrated that, in this mode, the $\mu 1$ channel usually opens only once before inactivating. The ensemble average of mode 1 sweeps displayed a rapid rise and prompt decay of current.

Examination of records from the F1304Q channel also revealed two distinct gating modes, although neither resembled the mode 1 gating seen in wild-type channels (Fig. 6A). In the dominant mode, which comprised 85% of the sweeps in this long run, the channel had a high open probability, with discrete openings and closures that persisted to the end of the sweep (Fig. 6 *C*). The second mode was a high open-probability burst mode, characterized by rapid gating transitions and a mean burst closed time of less than 1 ms (as described above; Fig. 6 *A* and *B*). Typically, the burst started immediately upon membrane depolarization and later during the sweep switched to a low-activity nonburst mode for the remainder of the 100-ms pulse.

Effect of coexpression of the β_1 subunit with $\mu 1$-F1304Q

In whole-cell recordings of the $\mu 1$ channel in *Xenopus* oocytes, coexpression of the rat brain β_1 subunit accelerates the time courses of macroscopic activation and inactivation (Isom et al., 1992; Cannon et al., 1993). To assess whether the gating changes observed in the $\mu 1$-F1304Q channel might be produced by altered interaction with the β_1 subunit, we coexpressed these two subunits in oocytes at a molar ratio of 1:1 (α:β_1). Upon step depolarizations to -20 mV, the most striking change was a marked reduction in the frequency of bursting mode sweeps relative to $\mu 1$-F1304Q expressed alone. During 1200 sweeps in a run from a one-channel patch containing $\mu 1$-F1304Q+β_1, channel gating consisted of discrete nonbursting openings and closures

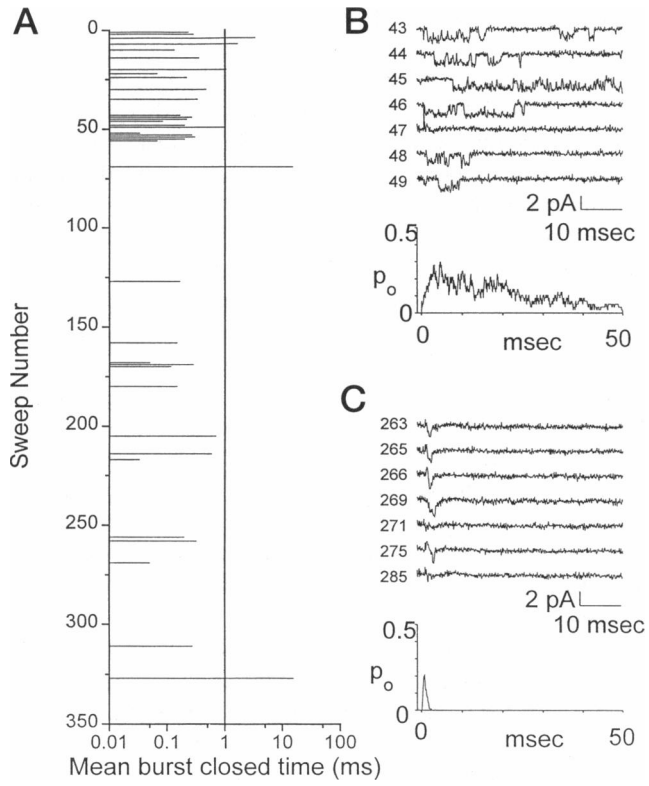

FIGURE 5 Modal gating in the μ1 sodium channel. (*A*) A diary of the mean burst closed time for the first two closures from sweeps having at least three openings in a one-channel patch depolarized at a repetition rate of 0.67 Hz from a holding potential of −120 mV to a test potential of −20 mV. A mean burst closing time of ≤1 m (*vertical line*) defines a mode 2 sweep. Sweeps with a longer mean burst closing time or with fewer than three openings were defined as mode 1. (*B*) Representative single-channel sweeps from mode 2 and the ensemble-average open probability. The sweep number is indicated to the left of the tracing. The ensemble average from this nondominant gating mode has a slowed decay of current. (*C*) Representative sweeps from the dominant gating mode 1 and an ensemble-average open probability generated from mode 1 sweeps. This ensemble average demonstrates the rapid current decay seen in native wild-type sodium channels.

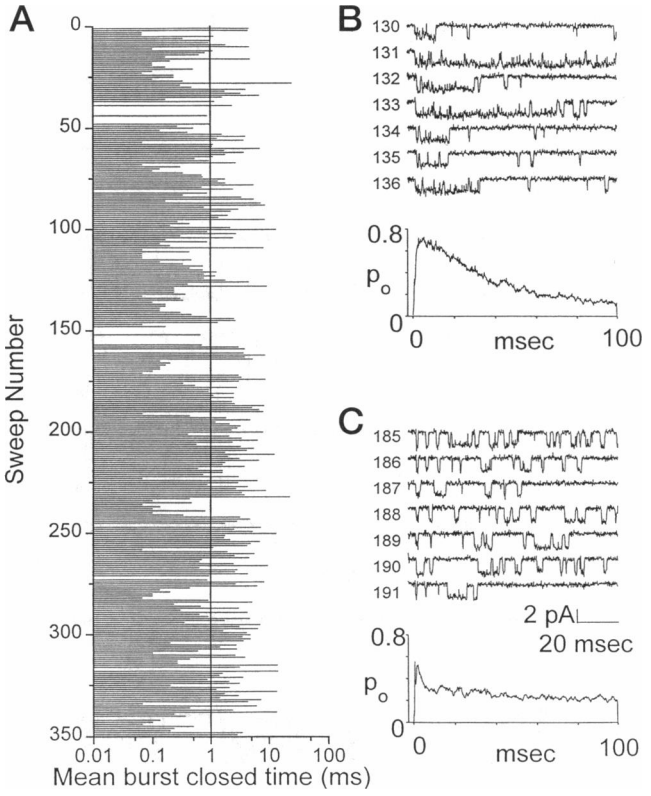

FIGURE 6 Modal gating in the μ1-F1304Q sodium channel. (*A*) A diary of the mean burst closed time for the first two closures from sweeps having at least three openings in a one-channel patch depolarized at a repetition rate of 0.67 Hz from a holding potential of −120 mV to a test potential of −20 mV. A mean burst closing time of ≤1 ms (*vertical line*) defines a bursting mode sweep. The total number of sweeps was 1000; the diary shows the first 350 sweeps to contrast with Fig. 5. (*B*) Selected consecutive sweeps during the bursting mode. The sweep number is indicated to the left of the tracing. The ensemble average was constructed from all bursting mode sweeps in the run. (*C*) Selected consecutive sweeps during the nonbursting mode. The ensemble average was constructed from all mode 1 sweeps.

for 98.8% of the sweeps (Fig. 7 *A*). Only rare scattered sweeps displayed the rapid burst mode seen more commonly with μ1-F1304Q expressed alone (Fig. 7 *A*, last sweep). This behavior was observed in two additional patches. The relative absence of bursting confirmed that the β_1 subunit was being coexpressed.

We then considered whether, in addition to reducing the frequency of the rapid burst mode, β_1 coexpression altered the kinetics of the nonbursting mode. The mean open times for the nonbursting μ1-F1304Q+β_1 channels (2.3 ± 0.3 ms; $N = 3$) were slightly longer than those recorded in nonbursting μ1-F1304Q channels (1.9 ± 0.1 ms), but the difference was not statistically significant ($p > 0.05$). The ensemble current (Fig. 7 *B*) and the normalized first latency histogram (Fig. 7 *C*) generated from the nonbursting μ1-F1304Q+β_1 channels demonstrated an acceleration of activation that is characteristic of β_1 coexpression with wild-type sodium channel α subunits in oocytes (Isom et al., 1992; Cannon et al., 1993). In comparison with the ensemble current for the nonbursting mode of μ1-F1304Q (Fig. 7B, dashed curve), the time course of current decay for μ1-F1304Q+β_1 is further slowed by β_1 coexpression. These findings indicate that β_1 coexpression stabilizes the dominant nonbursting mode of μ1-F1304Q, accelerates activation of the channel, and has modest effects on the decay kinetics of ensemble currents. Therefore, the predominant effect of the F1304Q mutation is a change in gating that markedly slows macroscopic current decay independently of interactions with the β_1 subunit.

Markov model for the μ1 and the μ1-F1304Q channels

To gain further insight into the gating changes produced by the μ1-F1304Q mutation we derived rate constants for multistate Markov models for μ1 and for μ1-F1304Q from ensemble-average currents and single-channel data, using

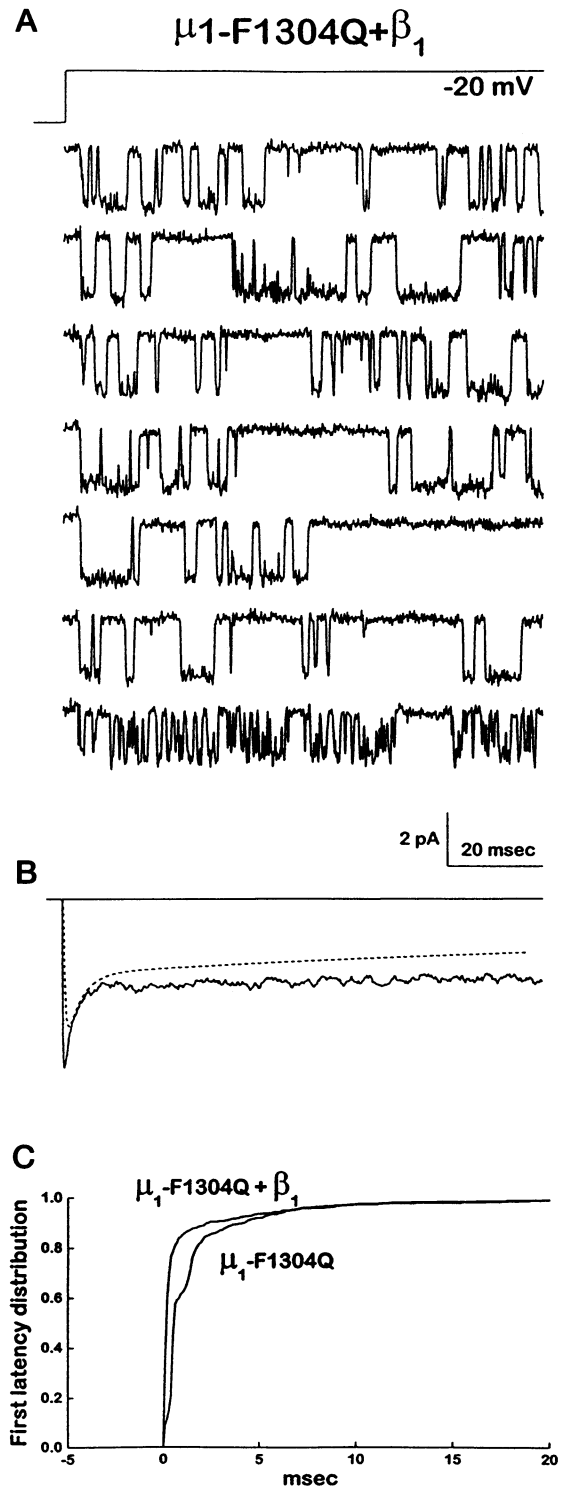

FIGURE 7 Coexpression of μ1-F1304Q and the β_1 subunit. (*A*) Representative single-channel records from a one-channel patch depolarized at a repetition rate of 0.67 Hz from a holding potential of −120 mV to a test potential of −20 mV. The last sweep is one of only 15 of 1200 sweeps that exhibited a high open probability burst mode. (*B*) Ensemble current generated from 1200 consecutive sweeps. The dashed curve is the model fit for μ1-F1304Q without β_1 coexpression. (*C*) First latency distribution for nonbursting sweeps from this patch compared with that from a patch containing μ1-F1304Q alone. The data sets were normalized by removing sweeps without openings to allow direct comparison of the times to first openings.

an iterative numerical approach. Inasmuch as the F1304Q mutation is at a site believed to mediate fast inactivation of the sodium channel, the gating model for the mutant channel was configured to be identical to the wild-type model, except for the rate constants to and from the fast-inactivated state (I_1). The models aimed to reproduce the dominant nonbursting mode in both the μ1 and the μ1-F1304Q channels during step depolarizations to −20 mV. The gating transitions in the bursting modes for both channels were not well resolved, and therefore quantitative modeling of these modes was not attempted. Because traces with burst activity accounted for only 15% of the records in a long run, our model reproduced the general behavior of the μ1-F1304Q channel independently of the modal gating.

The model was constrained by the following observations: A single open state was defined because all open time histograms were well fitted by single exponential functions. In whole-cell recordings, decay of peak current and recovery from inactivation curves are best fitted with a minimum of two exponential functions, and therefore the model incorporated two inactivated states (Ji et al., 1994; Brown et al., 1981; Follmer et al., 1987). The measured mean open times at −20 mV (0.38 ms for μ1 and 2.0 ms for μ1-F1304Q) were used to constrain the reciprocal of the sum of the rate constants leaving the open state in the models ($1/\delta + 1/k_8 + 1/k_4$).

With these conditions incorporated into the fitting algorithm, the model and rate constants shown in Figs. 8 *A* and *B* were generated; only the rate constants for entry to and exit from OI_1 (k_1, k_2, k_3, k_4) were different for μ1 and for μ1-F1304Q. This model closely reproduced the upstroke and the decay of peak current for both μ1 and μ1-F1304Q (Fig. 9 *B*, left and middle panels) and the slower decay of current during the maintained plateau in μ1-F1304Q. The major differences between the currents are the markedly faster current decay and the reduced peak open probability for μ1 relative to μ1-F1304Q. One can further understand these effects from the model by reviewing the inactivation rate constants and the time course of occupancy of the two inactivated states for each of the channels. For μ1, occupancy of both inactivated states develops rapidly; at steady state, the OI_1 occupancy is ~72% and the OI_2 occupancy is ~28% (Fig. 9 *A*, left panel). The higher on-rate for fast-inactivation particle binding (k_4) relative to slow-inactivation particle binding (k_8) accounts for the preference of OI_1 rather than OI_2. For μ1-F1304Q, k_4 is markedly slower (251 s^{-1} as opposed to 2533 s^{-1} for μ1) and k_3, the rate constant for unbinding of the fast inactivation particle, is accelerated (165 s^{-1} for μ1-F1304Q and near zero for μ1) such that the on- and off-rates for binding of the fast-inactivation particle are similar in magnitude. Thus, OI_1 is no longer an absorbing state, and the channel readily reopens from it. This is consistent with the slow decay of peak current in whole-cell recordings and with the multiple-channel reopenings observed in single-channel recordings. Entry into OI_1 is slower for μ1-F1304Q and accounts for the prolongation of the mean open time.

A

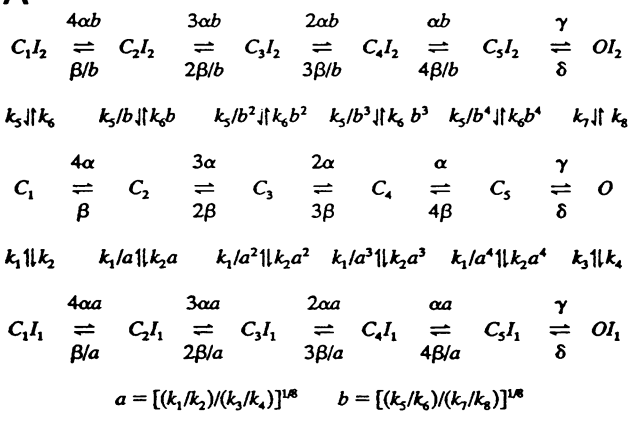

B

sec^{-1}	k5	k6	k7	k8
μ1	0.001	≈0	1.29	9.92
μ1-F1304Q	0.001	≈0	1.29	9.92
μ1-F1304Q + β_1	0.5x10^{10}	≈0	252	111
	α	β	γ	δ
μ1	3827	911	6.3x10^{10}	314
μ1-F1304Q	3827	911	6.3x10^{10}	314
μ1-F1304Q + β_1	9516	2001	0.5x10^{10}	273
	k1	k2	k3	k4
μ1	≈0	0.02	≈0	2533
μ1-F1304Q	3096	1.62	165	251
μ1-F1304Q + β_1	3096	1.62	165	251

FIGURE 8 Markov models for the μ1, μ1-F1304Q, and μ1-F1304Q+β_1 sodium channels. (*A*) Schematic of the model with four independent and identical gating sensors along the activation pathway and two independent inactivation gating particles (OI_1 and OI_2). (*B*) Rate constants derived from best fits of the model to μ1, μ1-F1304Q, and μ1-F1304Q+β_1 ensemble currents at −20 mV.

Over time, channels gradually and progressively enter the OI_2 state, which has a lower on-rate (9.92 versus 251 s^{-1}) and an even lower off-rate (1.29 versus 165 s^{-1}) relative to OI_1. Redistribution of channels into OI_2 from the OI_1 and open states accounts for the gradual decay of the μ1-F1304Q ensemble-average current. The increase in peak open probability seen in the μ1-F1304Q channel develops as a consequence of decreased fast inactivation (I_1) from closed states relative to μ1. The on-rate for fast-inactivation particle binding to the C_5 state (k_2a^4) is 26,947 s^{-1} for μ1 and 87 s^{-1} for μ1-F1304Q. This difference also accounts for the relative infrequency of null sweeps in μ1-F1304Q channels.

Markov model for the μ1-F1304Q+β_1 channel

The primary effect of β_1 coexpression on wild-type μ1 channels is to stabilize a nonbursting mode of the channel (Zhou et al., 1991), an effect that we also observe when β_1 is coexpressed with μ1-F1304Q. However, when only the nonbursting sweeps were considered, β_1 coexpression caused acceleration of activation and slowed the decay of the ensemble current. Because there was no significant change in mean open time by β_1 coexpression, we hypothesize that the β_1 subunit has no direct influence on fast inactivation of the μ1-F1304Q channel. Therefore, we applied the previously described Markov model to fit the ensemble current for the μ1-F1304Q+β_1 channel, employing the rate constants for transitions involving the fast-inactivated state (k_1, k_2, k_3, and k_4) that were derived for the μ1-F1304Q channel. The other rate constants were not constrained other than by the mean open time for the channel at −20 mV. As shown in Fig. 9 *B* (right panel), the minimized least-squares fit closely reproduced the rapid activation of the μ1-F1304Q+β_1 channel, the initial rapid decay of peak current, and the very slowly decaying plateau current. Compared with the μ1-F1304Q model, coexpression of the β_1 subunit increases rate constant α by 3.2-fold to speed activation and reduces the ratio of rate constants k_8/k_7 from 7.7 to 0.4 to equilibrate more nearly the rates of entry into and exit from the slow inactivated state (OI_2). As a result, at steady state, OI_2 is less absorbing and the decay of ensemble current is slowed.

DISCUSSION

Fast inactivation of the voltage-gated sodium channel is mediated by translocation of a segment of the intracellular linker between homologous domains III and IV and subsequent binding to a site within the inner vestibule of the channel. A triplet of hydrophobic amino acids (isoleucine–phenylalanine–methionine) near the amino-terminal end of this linker appears to form the blocking particle (West et al., 1992). Mutation of any one of these three residues to a more hydrophilic residue results in slowing of the decay of whole-cell current. In the rat brain IIA sodium channel this effect is most dramatic when the phenylalanine at position 1489 is modified. We studied a mutation (F1304Q) at the analogous location in the μ1 rat skeletal muscle sodium channel, using single-channel, cell-attached patch-clamp recordings in *Xenopus* oocytes to define the changes in gating that are responsible for delayed inactivation of whole-cell currents.

As expected from its location on the cytoplasmic side of the channel, the μ1-F1304Q mutation does not alter unitary current amplitude or slope conductance and thus does not have a significant effect on permeation properties. The changes in gating, however, are readily apparent from inspection of single-channel records. The μ1-F1304Q currents have longer openings and more frequent reopenings at membrane potentials above −60 mV relative to wild-type

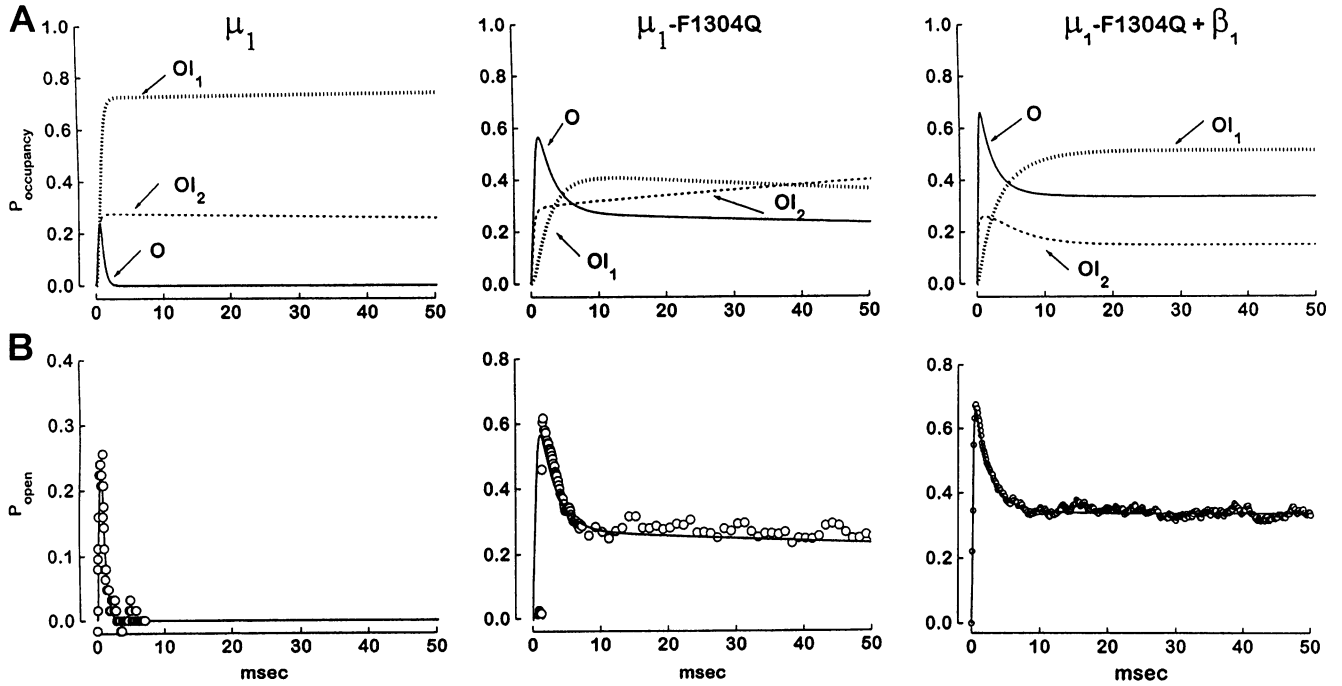

FIGURE 9 State occupancy and fit of Markov models to data. (*A*) Time course of occupancy of the open and inactivated states for μ1, μ1-F1304Q, and μ1-F1304Q+β_1. (*B*) Ensemble-average open probabilities (*symbols*) and predicted curves from the Markov model (*curves*). The data include only the dominant nonburst mode sweeps.

currents. In the wild-type sodium channel, mean open time progressively lengthens as membrane potential becomes more depolarized up to approximately 0 mV but then shortens at more positive test potentials (Fig. 4). This biphasic voltage dependence of mean open time is absent in μ1-F1304Q. The delay in inactivation in μ1-F1304Q results primarily from frequent reopenings of the channel. Both the wild-type and the mutant channels exhibited a dominant gating mode with well-resolved openings and a less frequent gating mode characterized by high open-probability bursts with poorly resolved openings. The two modes were distinguished by the presence or absence of an initial burst of three openings separated by closed times of less than 1.0 ms.

We predicted that the composite changes in gating produced by the F1304Q mutation could be attributed to a selective modification of fast inactivation rather than to a more global change in kinetics, altered modal gating, or a change in the interaction between the α and β_1 subunits. Slowed entry into an inactivated state from the open state would prolong open times, and this effect would be more pronounced at positive membrane potentials, where channel openings are increasingly terminated by transitions to an absorbing inactivated state (Yue et al., 1989; Scanley et al., 1990; Berman et al., 1990). Transitions from inactivated states back to the open state, as a result of defective inactivation, could account for the increased frequency of reopenings and the delayed decay of macroscopic current. To test this hypothesis we developed a model (Tomaselli et al., 1995) similar to that described by Kuo and Bean (1994) for neuronal sodium channels. Our model includes a second inactivation particle because recovery from inactivation is described by at least two time constants (Ji et al., 1994; Brown et al., 1981; Follmer et al., 1987). Constrained only by mean open-time measurements, the model was challenged to fit simultaneously ensemble-average currents from μ1 and μ1-F1304Q at −20 mV. All rate constants, except those to and from the OI_1 state, were identical. As shown in Fig. 9, the model closely reproduced both the activation and the inactivation kinetics for μ1 and μ1-F1304Q. As has been observed for mutations at analogous positions in the rat brain (rBIIA) and human heart (hH1) sodium channels, the F1304Q mutation in skeletal muscle sodium channels has no effect on the activation pathway (West et al., 1992; Hartmann et al., 1994).

Coexpression of μ1-F1304Q+β_1 stabilized the dominant nonbursting mode and accelerated activation of the channel. The ensemble behavior of these patches was consistent with that observed in whole-cell experiments, and we believe that our limited single-channel data with β_1 coexpression are valid and complementary to the data for the α subunit expressed alone. Mean open times were not significantly changed by β_1 coexpression, and the μ1-F1304Q model rate constants to and from the fast-inactivated state (OI_1) could be directly inserted into the model for μ1-F1304Q+β_1. Therefore the changes in fast inactivation attributed to the F1304Q mutation appear to be independent of any altered interaction between the α and β_1 subunits. The further slowing of decay with β_1 coexpression was simulated by a modification in the OI_2 slow-inactivation rate constants.

Changes in these slow transitions have a relatively minor influence on the mean open time, as we observed experimentally.

The slowed decay of macroscopic current, the increased mean open time, and the more frequent reopenings observed in μ1-F1304Q than in μ1 single-channel recordings can be explained by a selective effect on fast inactivation. This suggests that the gate remains intact and retains the ability to occlude the pore but forms a less-stable hydrophobic interaction with its docking site because of the replacement of phenylalanine by a hydrophilic residue. Rather than being absorbing, the OI_1 state in μ1-F1304Q is one from which the channel readily reopens. Not only does the inactivation gate bind less avidly but the on-rate constant for the O-to-OI_1 transition (k_4) is more than an order of magnitude slower than that for the μ1 channel. These observations reinforce the notion that the μ1-F1304Q channel is inactivation defective rather than inactivation deficient. Transitions to and from OI_2 do not appear to be influenced by the F1304Q mutation during mode 1 gating. Therefore, slow inactivation remains intact, and gradual occupancy of this absorbing state accounts for the slow, steady decay of macroscopic current. Similar changes in the rate constants to inactivated states have been seen with an F–Q mutation at an analogous site in the human heart (hH1) channel (Hartmann et al., 1994). Although it is qualitatively similar to ours, this model incorporated two serial inactivated states rather than two independent inactivation particles, was not constrained by single-channel data, and did not examine the influence of β_1 subunit coexpression. Furthermore, modal gating that has been observed prominently in rat brain sodium channels (Moorman et al., 1990) and skeletal muscle (Zhou et al., 1991; Ji et al., 1994) was not observed in the human heart sodium channels with the F–Q mutation (Hartmann et al., 1994). Nevertheless, such channels clearly exhibit modal gating with other mutations in the III–IV linker (Bennett et al., 1995). Mutations, such as μ1-F1304Q, that involve the IFM cluster selectively modify fast inactivation without altering activation kinetics. This occurs presumably by influencing only the hydrophobic interaction of the inactivation particle with its receptor and suggests that the basic molecular mechanism underlying fast inactivation is extremely well conserved across the family of voltage-gated sodium channels.

This research was supported by National Institutes of Health grants T32 HL07227 (D.W.O. and H.B.N.), RO1 HL50411 (G.F.T.), RO1 HL52768 (E.M.), and K11 HL02639 (J.H.L.), by the American Heart Association (J.R.B.) and the Passano Foundation (J.R.B.), and by a grant from the Whitaker Foundation (J.H.L.).

REFERENCES

Aldrich, R. W., D. P. Corey, and C. F. Stevens. 1983. A reinterpretation of mammalian sodium channel gating based on single channel recording. *Nature (Lond.).* 306:436–441.

Backx, P. B., D. T. Yue, J. H. Lawrence, E. Marban, and G. F. Tomaselli. 1992. Molecular localization of an ion-binding site within the pore of mammalian sodium channels. *Science.* 257:248–251.

Balser, J. R., P. B. Bennett, and D. M. Roden. 1990a. Time-dependent outward current in guinea pig ventricular myocytes: gating and kinetics of the delayed rectifier. *J. Gen. Physiol.* 96:835–863.

Balser, J. R., D. M. Roden, and P. B. Bennett. 1990b. Global parameter optimization for cardiac potassium channel gating models. *Biophys. J.* 57:433–444.

Bennett, P. B., K. Yazawa, N. Makita, and A. L. George. 1995. Molecular mechanism for an inherited cardiac arrhythmia. *Nature (Lond.).* 376: 683–685.

Berman, M. F., J. S. Camardo, R. B. Robinson, and S. A. Siegelbaum. 1990. Single sodium channels from canine ventricular myocytes: voltage dependence and relative rates of activation and inactivation. *J. Physiol.* 415:503–531.

Brown, A. M., K. S. Lee, and T. Powell. 1981. Sodium current in single rat heart muscle cells. *J. Physiol.* 318:479–500.

Cannon, S. C., A. I. McClatchey, and J. F. Gusella. 1993. Modification of the Na^+ current conducted by the rat skeletal muscle α subunit by coexpression with a human brain β subunit. *Pflügers Arch.* 423: 155–157.

Colquhoun, D., and F. J. Sigworth. 1983. Fitting and statistical analysis of single-channel records. *In* Single-Channel Recording. B. Sakmann and E. Neher, editors. Plenum Press, New York.

Follmer, C. H., R. E. Ten Eick, and J. Z. Yeh. 1987. Sodium current kinetics in cat atrial myocytes. *J. Physiol.* 384:169–197.

Grant, A. O., and C. F. Starmer. 1987. Mechanisms of closure of cardiac sodium channels in rabbit ventricular myocytes: single-channel analysis. *Circ. Res.* 60:897–913.

Hartmann, H. A., A. A. Tiedeman, S. F. Chen, A. M. Brown, and G. E. Kirsch. 1994. Effects of III-IV linker mutations on human heart Na^+ channel inactivation gating. *Circ. Res.* 75:114–122.

Hindmarsh, A. C. 1983. Odepack, a systematized collection of ode solvers. *In* Scientific Computing. R. S. Stepleman, editor. North-Holland Publishing Company, Amsterdam. 55–64.

Isom, L. L., K. S. Dejongh, D. E. Patton, B. F. X. Reber, J. Offord, H. Charbonneau, K. Walsh, A. L. Goldin, and W. A. Catterall. 1992. Primary structure and functional expression of the β_1 subunit of the rat brain sodium channel. *Science.* 256:839–842.

Isom, L. L., T. Scheuer, A. B. Brownstein, D. S. Ragsdale, B. J. Murphy, and W. A. Catterall. 1995. Functional co-expression of the beta 1 and type IIA alpha subunits of sodium channels in a mammalian cell line. *J. Biol. Chem.* 270:3306–3312.

Ji, S., W. J. Sun, A. L. George, R. Horn, and R. L. Barchi. 1994. Voltage-dependent regulation of modal gating in the rat SkM1 sodium channel expressed in *Xenopus* oocytes. *J. Gen. Physiol.* 104:625–643.

Kunkel, T. A., J. D. Roberts, and R. A. Zakour. 1987. Rapid and efficient site-specific mutagenesis without phenotypic selection. *Methods Enzymol.* 154:367–383.

Kuo, C. C., and B. P. Bean. 1994. Na^+ channels must deactivate to recover from inactivation. *Neuron.* 12:819–829.

McPhee, J. C., D. S. Ragsdale, T. Scheuer, and W. A. Catterall. 1994. A mutation in segment IVS6 disrupts fast inactivation of sodium channels. *Proc. Natl. Acad. Sci. USA.* 91:12346–12350.

McPhee, J. C., D. S. Ragsdale, T. Scheuer, and W. A. Catterall. 1995. A critical role for transmembrane segment IVS6 of the sodium channel alpha subunit in fast inactivation. *J. Biol. Chem.* 270:12025–12034.

Mitrovic, N., A. L. George, R. Heine, S. Wagner, U. Pika, U. Hartlaub, M. Zhou, H. Lerche, C. Fahlke, and F. Lehmann-Horn. 1994. K^+-aggravated myotonia: destabilization of the inactivated state of the human muscle Na^+ channel by the V1589 M mutation. *J. Physiol.* 478:395–402.

Moorman, J. R., G. E. Kirsch, A. M. J. VanDongen, R. H. Joho, and A. M. Brown. 1990. Fast and slow gating of sodium channels expressed by a single mRNA. *Neuron.* 4:243–252.

Nelder, J. A., and R. Mead. 1965. A simplex method for function minimization. *Comput. J.* 7:308–313.

Patton, D. E., J. W. West, W. A. Catterall, and A. L. Goldin. 1992. Amino acid residues required for fast Na^+-channel inactivation: charge neutral-

izations and deletions in the III–IV linker. *Proc. Natl. Acad. Sci. USA.* 89:10905–10909.

Petzold, L. R. 1983. Automatic selection of methods for solving stiff and nonstiff systems of ordinary differential equations. *SIAM J. Sci. Stat. Computing.* 4:136–148.

Scanley, B. E., D. A. Hanck, T. Chay, and H. A. Fozzard. 1990. Kinetic analysis of single sodium channels from canine cardiac Purkinje cells. *J. Gen. Physiol.* 95:411–437.

Stühmer, W., F. Conti, H. Suzuki, X. Wang, M. Noda, N. Yahagi, H. Kubo, and S. Numa. 1989. Structural parts involved in activation and inactivation of the sodium channel. *Nature (Lond.).* 339:597–603.

Tomaselli, G. F., N. Chiamvimonvat, H. B. Nuss, J. B. Balser, M. T. Perez-Garcia, R. H. Xu, D. W. Orias, P. H. Backx, and E. Marban. 1995. A mutation in the pore of the sodium channel alters gating. *Biophys. J.* 68:1814–1827.

Tomaselli, G. F., J. T. McLaughlin, M. E. Jurman, E. Hawrot, and G. Yellen. 1991. Mutations affecting agonist sensitivity of the nicotinic acetylcholine receptor. *Biophys. J.* 60:721–727.

Trimmer, J. S., S. S. Cooperman, S. A. Tomiko, J. Zhou, S. M. Crean, M. B. Boyle, R. G. Kallen, Z. Sheng, R. L. Barchi, F. J. Sigworth, R. H. Goodman, W. S. Agnew, and G. Mandel. 1989. Primary structure and functional expression of a mammalian skeletal muscle sodium channel. *Neuron.* 3:33–49.

Vandenberg, C. A., and R. Horn. 1984. Inactivation viewed through single sodium channels. *J. Gen. Physiol.* 84:535–564.

Vassilev, P. M., T. Scheuer, and W. A. Catterall. 1988. Identification of an intracellular peptide segment involved in sodium channel inactivation. *Science.* 241:1658–1661.

Vassilev, P. M., T. Scheuer, and W. A. Catterall. 1989. Inhibition of inactivation of single sodium channels by a site-directed antibody. *Proc. Natl. Acad. Sci. USA.* 86:8147–8151.

West, J. W., D. E. Patton, T. Scheuer, Y. Wang, A. L. Goldin, and W. A. Catterall. 1992. A cluster of hydrophobic amino acid residues required for fast Na^+-channel inactivation. *Proc. Natl. Acad. Sci. USA.* 89: 10,910–10,914.

Yue, D. T., J. H. Lawrence, and E. Marban. 1989. Two molecular transitions influence cardiac sodium channel gating. *Science.* 244:349–352.

Zhou, J., J. F. Potts, J. S. Trimmer, W. S. Agnew, and F. J. Sigworth. 1991. Multiple gating modes and the effect of modulating factors on the μ1 sodium channel. *Neuron.* 7:775–785.